



Case Report

# In Vivo Measurements of Transcranial Electrical Stimulation in Lesioned Human Brain: A Case Report

Hongjie Jiang <sup>1,2,†</sup>, Minmin Wang <sup>3,4,5,†</sup> , Dan Wu <sup>3,4</sup>, Jianmin Zhang <sup>1,2,4,\*</sup> and Shaomin Zhang <sup>3,5,\*</sup> 

<sup>1</sup> Department of Neurosurgery, The Second Affiliated Hospital, Zhejiang University School of Medicine, Hangzhou 310030, China

<sup>2</sup> Clinical Research Center for Neurological Diseases of Zhejiang Province, Hangzhou 310030, China

<sup>3</sup> Key Laboratory of Biomedical Engineering of Education Ministry, Department of Biomedical Engineering, School of Biomedical Engineering and Instrument Science, Zhejiang University, Hangzhou 310027, China

<sup>4</sup> Binjiang Institute of Zhejiang University, Hangzhou 310051, China

<sup>5</sup> Qiushi Academy for Advanced Studies, Zhejiang University, Hangzhou 310027, China

\* Correspondence: zjm135@zju.edu.cn (J.Z.); shaomin@zju.edu.cn (S.Z.)

† These authors contributed equally to this work.

**Abstract:** Transcranial electrical stimulation (tES) has been utilized widely in populations with brain lesions, such as stroke patients. The tES-generated electric field (EF) within the brain is considered as one of the most important factors for physiological effects. However, it is still unclear how brain lesions may influence EF distribution induced by tES. In this case study, we reported in vivo measurements of EF in one epilepsy participant with brain lesions during different tES montages. With the in vivo EF data measured by implanted stereo-electroencephalography (sEEG) electrodes, the simulation model was investigated and validated. Our results demonstrate that the prediction ability of the current simulation model may be degraded in the lesioned human brain.

**Keywords:** transcranial electrical stimulation; head model; in vivo; brain lesion; stereo-electroencephalography



**Citation:** Jiang, H.; Wang, M.; Wu, D.; Zhang, J.; Zhang, S. In Vivo Measurements of Transcranial Electrical Stimulation in Lesioned Human Brain: A Case Report. *Brain Sci.* **2022**, *12*, 1455. <https://doi.org/10.3390/brainsci12111455>

Academic Editors: Andrea Guerra and Caterina Cinel

Received: 12 September 2022

Accepted: 21 October 2022

Published: 27 October 2022

**Publisher's Note:** MDPI stays neutral with regard to jurisdictional claims in published maps and institutional affiliations.



**Copyright:** © 2022 by the authors. Licensee MDPI, Basel, Switzerland. This article is an open access article distributed under the terms and conditions of the Creative Commons Attribution (CC BY) license (<https://creativecommons.org/licenses/by/4.0/>).

## 1. Introduction

Transcranial electrical stimulation (tES), as a promising non-invasive brain stimulation technique, has been widely utilized in various neuropsychiatric research, such as stroke rehabilitation [1,2] and epilepsy [3,4]. However, the clinical efficacy of tES is still inconsistent and varies substantially across subjects in practice [5,6]. EF generated by tES within the target brain regions is one of the most significant factors for physiological effects [7,8]. In addition, because individual brain lesions have different morphologies and tissue dielectric properties compared to normal brain tissue, the influence on induced EF may be different from that of normal tissues [9]. The individual variability would be further exacerbated in populations with brain lesions [10]. However, owing to the limitation of clinical practical methods, EF distributions are not easy to record directly from human brains, especially in patients with brain lesions.

Thus, computational modeling of tES has been proposed to predict specific spatial EF distribution within the brain in a given individual [11]. It is a good visual and quantitative tool for investigating the substantial inter-individual variability in the lesioned brain. There have also been some reports about individualized stroke head models [9,12,13]. Johnstone et al. reported the effect of brain lesions on tDCS-induced EF under various lesion locations, distances, sizes, and conductivities in a head model. They found that the lesion characteristics have a substantial effect on tDCS-induced EFs, such as that lesions can alter the tDCS-induced EF magnitude in a target by 30%. Notwithstanding, it is still highly controversial as to whether the simulation models could reliably reflect the actual situation, especially for the lesioned brain [9,14]. The actual measurement of EF in vivo is very important for the validation and optimization of the simulation model.

Several studies have reported on the measurement of tES-generated voltage in patients with epilepsy [15–19] or Parkinson’s disease [20,21]. In a previous study, the validation of a simulation model was also performed via in vivo measurements in epilepsy patients [16], but their data mainly came from implanted ECoG electrodes; the results may be influenced by skull defects caused by electrode implantation [22]. However, so far, all of these in vivo measurements were conducted in the brain without lesions. In vivo clinical evidence is still lacking in brain lesions [23]. Studying the influence of lesions on tES via in vivo measurements would lay a solid foundation for future clinical optimizations.

In this case report, by using minimally invasive stereo-electroencephalography (sEEG) electrodes, we aim to conduct in vivo measurements of tES-induced EF in one epilepsy participant with brain lesions. Furthermore, the influence of brain lesions and electrode montage on EF were investigated, and the simulation model was validated with measured values.

## 2. Case Presentation

The participant was a 21-year-old, right-handed male who underwent sEEG recording to localize seizure foci for epilepsy surgery. As shown in Figure 1, he had two congenital malacia foci (yellow area in the right Figure 1B), one located in the left lateral middle and inferior frontal gyri, and the other located in the pars opercularis. His pre-implantation MRI data was acquired with a 3T MRI scanner (UIH Umr 790 system). The scanning parameters were TR = 8.2 ms, TE = 3.2 ms, flip angle = 12°. Post-implantation CT data were acquired with a CT scanner (SIEMENS SOMATOM Perspective, 237 mA/ slice, 120 kV). The scanning resolution of the MRI and CT images was  $0.5 \times 0.5 \times 1.0 \text{ mm}^3$ .

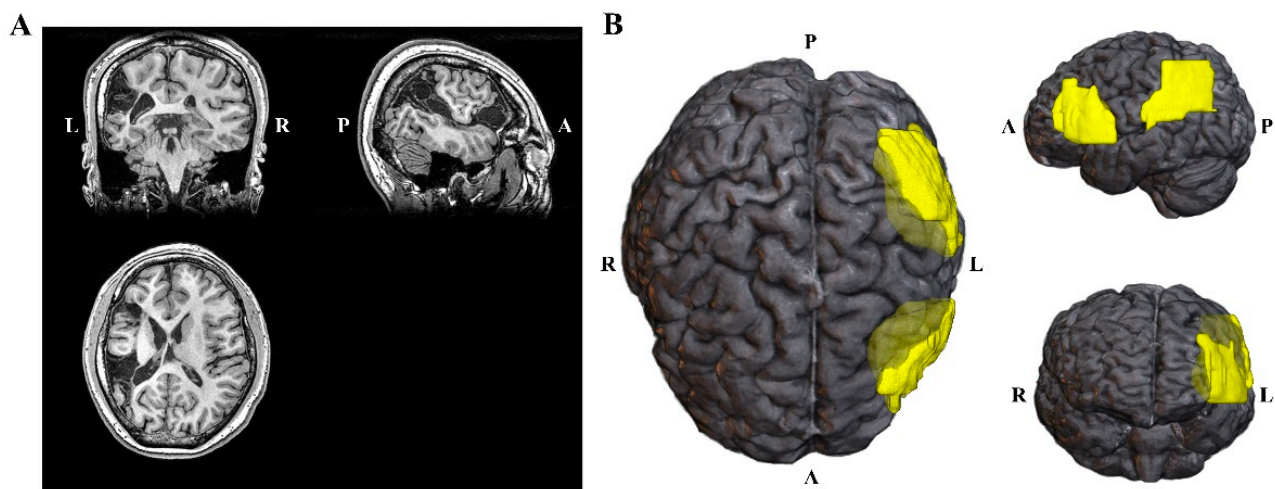


**Figure 1.** Three-dimensional (3D) MRI image and the locus of brain lesions. (A) T1-weighted MR brain images of participant. (B) Lesion map of participant, yellow areas represent brain lesions.

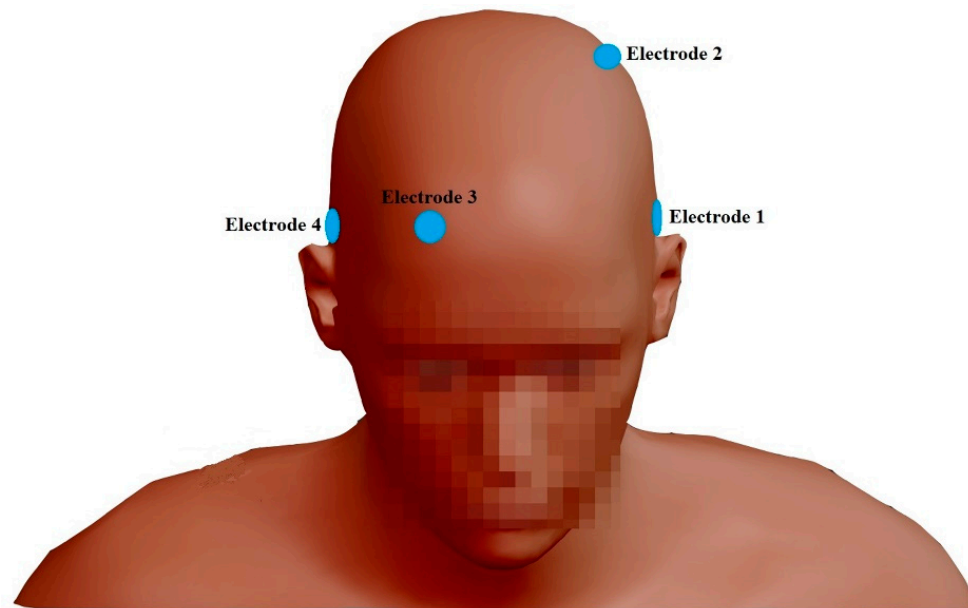
All clinical procedures were carried out in accordance with the Declaration of Helsinki. The Institutional Review Board at the Second Affiliated Hospital Zhejiang University School of Medicine approved the protocol (N2018-126). The participant has given his written consent before participating in the study.

## 3. Materials and Methods

### 3.1. Transcranial Alternating Current Stimulation

Four round Ag/AgCl electrodes ( $3.14 \text{ cm}^2$ , Pistim, Neuroelectronics, Barcelona, Spain) were attached to the scalp (T7, C3, Fp2, and T8, in order) and used in three different montages, as shown in Figure 2. At each stimulus trial, we applied transcranial alternating current stimulation (tACS) through two stimulation electrodes coated with a conductive gel

(HD-GEL, Soterix Medical, New York, NY, USA), using a StarStim8 system (Neuroelectronics, Barcelona, Spain).



*Montage-13*: Electrode 1 (0.5 mA), Electrode 3 (return electrode)

*Montage-14*: Electrode 1 (0.5 mA), Electrode 4 (return electrode)

*Montage-23*: Electrode 2 (0.5 mA), Electrode 3 (return electrode)

**Figure 2.** The positions of stimulation electrodes.

Prior to each trial, we recorded a rest condition for 30 s and then applied 0.5 mA stimulation at a frequency of 100 Hz for 2 min with 10 s ramp up and down periods. Post-stimulation was recorded for another 30 s. The inter-stimulus interval lasted more than 30 s. For safety considerations, the impedance of the electrodes was monitored throughout the experiment and was always lower than 10 k $\Omega$ .

### 3.2. Intracranial Recording Setup

Based on clinical diagnosis, 112 sEEG recording electrodes (Sinovation, China; 0.8 mm diameter, 3.5 mm contact spacing, 2 mm contact length) were inserted to record the intracranial voltage changes around the suspected seizure foci. The locations and the numbers for the electrode insertions were determined for clinical reasons. The common reference for the recordings was the average value of two clinically adjacent recording electrodes (Electrode A5 and A6, located at the right inferior frontal gyrus). The ground electrode was positioned in the right mastoid region. The signal was band-pass filtered (0.16–300 Hz) using a clinical amplifier (EEG-1200C, Nihon Kohden, Tokyo, Japan) at a ~2 kHz sampling rate, and further filtered using a narrow band (95–105 Hz), zero phase, second-order Butterworth IIR filter to reduce noise interference. The tACS-induced average peak voltages were used as the measured value for subsequent analysis.

### 3.3. Model Simulations

Our study adopted ROAST (Realistic Olumetric-Approach to Simulate Transcranial electric stimulation, ROAST 3.0, <https://www.parralab.org/roast/> (accessed on 6 April 2021)) [24] for electric fields modeling. The sEEG electrodes were not modeled in EFs modeling (Figure 3). All tissues (including brain lesions) were assumed to have isotropic conductivities (WM: 0.126 S/m, GM: 0.276 S/m, CSF: 1.65 S/m, skull: 0.01 S/m, scalp: 0.465 S/m, brain lesions: 0.80 S/m [25], air cavities:  $2.5 \times 10^{-14}$  S/m, electrode:  $5.9 \times 10^7$  S/m, gel: 0.3 S/m). The MRI image was co-registered with a CT image, and each of the

sEEG electrode locations were determined using Brainstorm software (brainstorm3, <https://neuroimage.usc.edu/brainstorm/> (accessed on 2 November 2020)) [26]. Simulated voltage was obtained by re-referencing the sEEG recordings with the common reference.

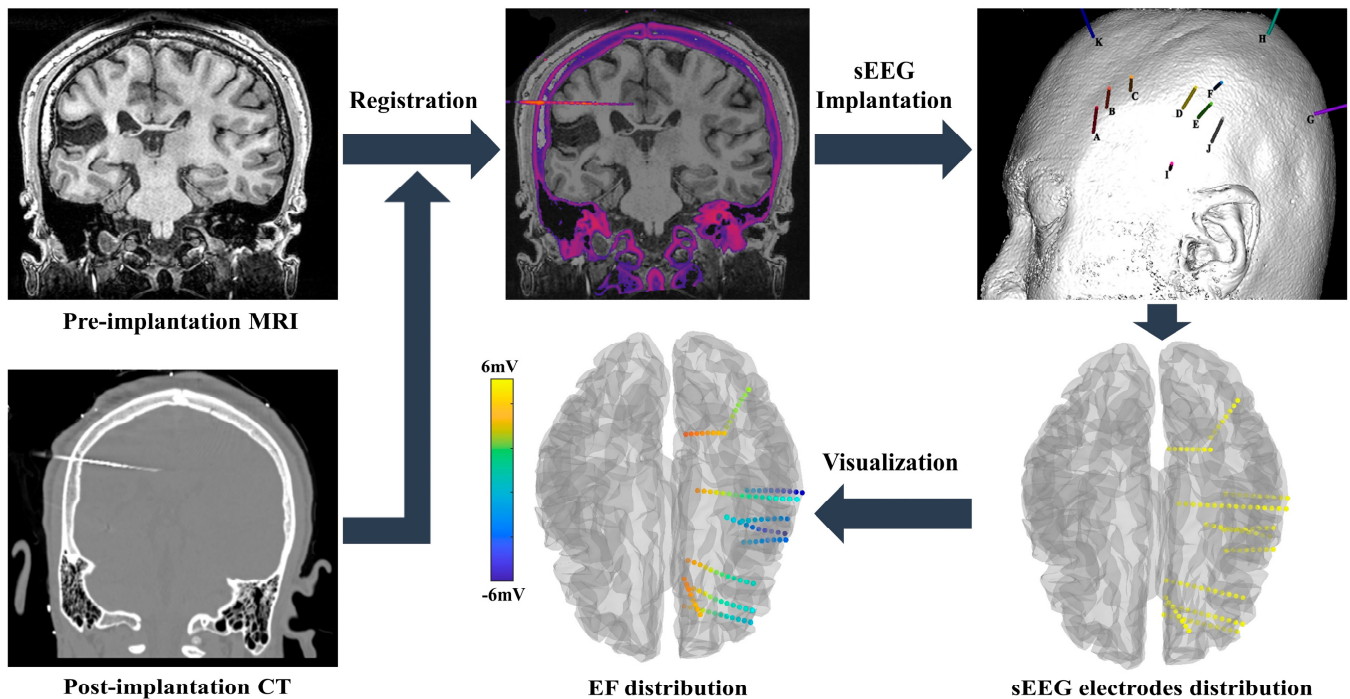


**Figure 3.** The analysis procedure of sEEG electrode positioning and Electric field modeling.

### 3.4. Data Analysis

For data analysis, the projected electric field for both the predicted and measured values, was calculated by subtracting voltage values from adjacent electrodes and dividing by their distance. The electric field component, along with the direction of the measurement electrodes (projection of the electric field), were then estimated. Based on the results above, correlations between the predicted and measured values were studied (Pearson correlation coefficient). Using linear regression, the simulation model was evaluated for its accuracy in estimating voltage distributions and EF distributions.

## 4. Measured and Simulated Electric Field of tES

To investigate the influence of the electrode montage and brain lesion on the EF, we compared the simulation results with measured values. As shown in Figure 4A, the recorded voltages were highly correlated with the simulated voltage values (Pearson correlation coefficient  $r = 0.97$ ,  $p < 0.001$ ; slope of the best linear fit  $s = 0.78$ ) under *Montage-13*. The spatial electric potential distributions from the recorded and simulated results for *Montage-13* are shown in Figure 4C. (The results for other montages are displayed in Figure S1.) As displayed in Figure 4B, we also found a moderate correlation between the measured and simulated values in the EF distributions ( $r = 0.58$ ,  $p < 0.001$ ;  $s = 0.44$ ). In line with several previous studies [16,27], we found a lower correlation between measured and simulated EF, in contrast to voltage values.



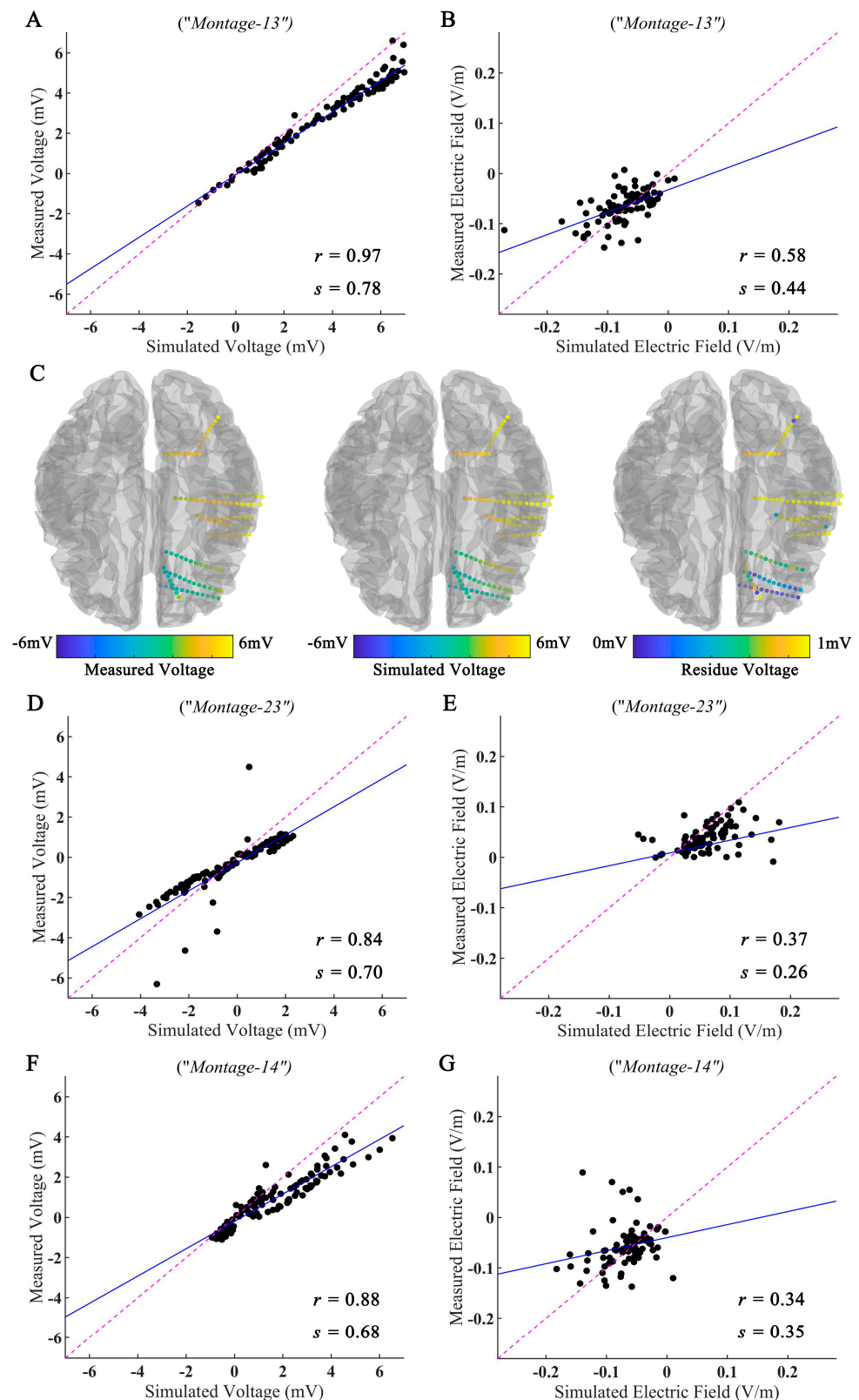


**Figure 4.** Measured and simulated electric fields of tES. (**A,B**) The measured voltages and projected electric fields with simulated values for *Montage-13*. (**C**) The spatial electric potential distributions from recorded and simulated voltages for *Montage-13*. (**D–G**) Measured and simulated results for *Montage-23* and *Montage-14*. Points falling on the magenta line represent perfect prediction (slope  $s = 1$ ). The blue line represents the fitting line.

Similar results were observed under *Montage-23* (Voltage:  $r = 0.84$ ,  $p < 0.001$ ,  $s = 0.70$ , Figure 4D; EF:  $r = 0.37$ ,  $p < 0.001$ ,  $s = 0.26$ , Figure 4E) and *Montage-14* (Voltage:  $r = 0.88$ ,  $p < 0.001$ ,  $s = 0.68$ , Figure 4F; EF:  $r = 0.34$ ,  $p < 0.001$ ,  $s = 0.35$ , Figure 4G).

## 5. Discussion

The case report, for the first time, provides direct evidence for tES-induced EF in the lesioned human brain. Several previous modeling studies have studied the effect of lesions on tES-induced EF [9,12–14,28–30]. These simulated results mainly explore the situation of stroke patients and have found that lesions caused a shunt of stimulation current in target areas. Although these simulation models have considered the effects of brain lesions, but have only provided computational results, it remains unclear as to how lesions may influence tES-induced EF within the brain. In this case report, our results show that the EF modeling can effectively predict EF distribution during tES in the lesioned brain under various electrical stimulation montages. The simulation model is also validated via in vivo measurement in previous studies of the non-lesioned brain [16,27]; they found a higher correlation between the simulated and predicted EF (Huang et al.:  $r = 0.89$ ; Wang et al.:  $r = 0.73$ ). These results indicated the influence of brain lesions on model performance. A variation in conductance may be one important factor. Lesions in the brain have a different conductance than healthy tissue [25], and the conductivity of different lesions is still unclear. In our simulation model, the conductivity of brain lesions (0.80 S/m) was assigned to be less than that of CSF (1.65 S/m). In our results, the simulated EF value seemed larger than the measured value, which may suggest that the conductivity value of the brain lesion is greater than 0.80 S/m. The EF is strongly influenced by large lesions that have a high assigned conductivity [12]. How to determine the conductivity of the lesion is essential for future research.

It is noteworthy that the correlation of EF was lower than that of the voltage value. The observed dispersion in the electric field may come from several factors: First, the projected electric field was calculated in the direction of adjacent recording channels by subtracting the voltage values and dividing by their distance; thus, the amplitude of the electric field is relatively small, and the correlation of EF was decreased compared to the voltage. Second, the sEEG electrodes were not modeled in our simulation model, and the electric field near the electrode may be disturbed. Third, the influence of environmental noise, electrode contact, and the signal amplifier. Fourth, the influence of spontaneous brain activities, although this itself is relative small compared to the magnitude of the tES-induced voltage (Figure S2).

Limited to the nature of the clinical trial, our study only involves one lesioned human brain. However, lesion characteristics are varied in different individuals, such as distance and size. When lesions are larger, or closer to the target brain areas, the induced EF would have the greatest impact [30]. Thus, the characteristics of the lesion would exacerbate inter-individual variability in the current delivery [12]. More subjects are needed in future studies to investigate these variables. In addition, the simulation model would be improved when sEEG electrodes are modeled in a simulation model [28]. Our in vivo measurements provided precious data for studying the influence of lesions on tES-induced EF, which could shed light on future studies.

**Supplementary Materials:** The following supporting information can be downloaded at: <https://www.mdpi.com/article/10.3390/brainsci12111455/s1>. Figure S1: (A) The spatial electric potential distributions from recorded and simulated voltages for *Montage-23*. (B) The spatial electric potential distributions from recorded and simulated voltages for *Montage-14*. Figure S2: Example of signal analysis from one sEEG electrode. (A) Raw data from one sEEG electrode. (B) Band-pass filtered signal. (C) The power spectrum at each stimulation stage. (D) Time-frequency analysis based on wavelet transform.

**Author Contributions:** H.J.: validation, formal analysis, investigation, writing—original draft. M.W.: study conceptualization, methodology, software, formal analysis, investigation, writing—original draft, visualization. D.W.: study conceptualization, writing—original draft. J.Z.: study conceptualization, resources, supervision, funding acquisition. S.Z.: study conceptualization, writing—original draft, resources, supervision, funding acquisition. All authors have read and agreed to the published version of the manuscript.

**Funding:** This research was funded by the Key Research and Development Program of Zhejiang Province (Grant number: 2021C03107, 2021C03003, 2021C03050 and 2022C03029), the Natural Science Foundation of Zhejiang Province (Grant number: LQ20H090012), the Program from the Health and Family Planning Commission of Zhejiang Province (Grant number: 2020KY134) and the Fundamental Research Funds for the Central Universities (Grant number: 2019FZJD005 and K20200185).

**Institutional Review Board Statement:** The study was conducted in accordance with the Declaration of Helsinki, and approved by the Institutional Review Board of the Second Affiliated Hospital Zhejiang University School of Medicine (protocol code N2018-126).

**Informed Consent Statement:** Informed consent was obtained from all subjects involved in the study.

**Data Availability Statement:** Data involved in this study are available upon reasonable request.

**Acknowledgments:** We would like to thank the participant for his generous support.

**Conflicts of Interest:** The authors declare no conflict of interest. The funders had no role in the design of the study; in the collection, analyses, or interpretation of data; in the writing of the manuscript; or in the decision to publish the results.

## References

1. Feil, S.; Eisenhut, P.; Strakeljahn, F.; Müller, S.; Nauer, C.; Bansi, J.; Weber, S.; Liebs, A.; Lefaucheur, J.-P.; Kesselring, J. Left Shifting of Language Related Activity Induced by Bihemispheric TDCS in Postacute Aphasia Following Stroke. *Front. Neurosci.* **2019**, *13*, 295. [\[CrossRef\]](#) [\[PubMed\]](#)
2. Chang, M.C.; Kim, D.Y.; Park, D.H. Enhancement of Cortical Excitability and Lower Limb Motor Function in Patients with Stroke by Transcranial Direct Current Stimulation. *Brain Stimul.* **2015**, *8*, 561–566. [\[CrossRef\]](#) [\[PubMed\]](#)
3. San-Juan, D.; Morales-Quezada, L.; Garduño, A.J.O.; Alonso-Vanegas, M.; González-Aragón, M.F.; López, D.A.E.; Gregorio, R.V.; Anschel, D.J.; Fregni, F. Transcranial Direct Current Stimulation in Epilepsy. *Brain Stimul.* **2015**, *8*, 455–464. [\[CrossRef\]](#) [\[PubMed\]](#)
4. Yang, D.; Wang, Q.; Xu, C.; Fang, F.; Fan, J.; Li, L.; Du, Q.; Zhang, R.; Wang, Y.; Lin, Y.; et al. Transcranial Direct Current Stimulation Reduces Seizure Frequency in Patients with Refractory Focal Epilepsy: A Randomized, Double-Blind, Sham-Controlled, and Three-Arm Parallel Multicenter Study. *Brain Stimul.* **2020**, *13*, 109–116. [\[CrossRef\]](#)
5. Regner, G.G.; Pereira, P.; Leffa, D.T.; De Oliveira, C.; Vercelino, R.; Fregni, F.; Torres, I.L. Preclinical to Clinical Translation of Studies of Transcranial Direct-Current Stimulation in the Treatment of Epilepsy: A Systematic Review. *Front. Neurosci.* **2018**, *12*, 189. [\[CrossRef\]](#)
6. Dong, K.; Meng, S.; Guo, Z.; Zhang, R.; Xu, P.; Yuan, E.; Lian, T. The Effects of Transcranial Direct Current Stimulation on Balance and Gait in Stroke Patients: A Systematic Review and Meta-Analysis. *Front. Neurol.* **2021**, *12*, 643. [\[CrossRef\]](#)
7. Rawji, V.; Ciocca, M.; Zacharia, A.; Soares, D.; Truong, D.; Bikson, M.; Rothwell, J.; Bestmann, S. TDCS Changes in Motor Excitability Are Specific to Orientation of Current Flow. *Brain Stimul.* **2018**, *11*, 289–298. [\[CrossRef\]](#)
8. Liu, A.; Vöröslakos, M.; Kronberg, G.; Henin, S.; Krause, M.R.; Huang, Y.; Opitz, A.; Mehta, A.; Pack, C.C.; Krekelberg, B. Immediate Neurophysiological Effects of Transcranial Electrical Stimulation. *Nat. Commun.* **2018**, *9*, 1–12. [\[CrossRef\]](#)
9. van der Crujisen, J.; Piastra, M.C.; Selles, R.W.; Oostendorp, T.F. A Method to Experimentally Estimate the Conductivity of Chronic Stroke Lesions: A Tool to Individualize Transcranial Electric Stimulation. *Front. Hum. Neurosci.* **2021**, *15*, 738200. [\[CrossRef\]](#)
10. Peterchev, A.V.; Wagner, T.A.; Miranda, P.C.; Nitsche, M.A.; Paulus, W.; Lisanby, S.H.; Pascual-Leone, A.; Bikson, M. Fundamentals of Transcranial Electric and Magnetic Stimulation Dose: Definition, Selection, and Reporting Practices. *Brain Stimul. Basic Transl. Clin. Res. Neuromodul.* **2012**, *5*, 435–453. [\[CrossRef\]](#)
11. Puonti, O.; Van Leemput, K.; Saturnino, G.B.; Siebner, H.R.; Madsen, K.H.; Thielscher, A. Accurate and Robust Whole-Head Segmentation from Magnetic Resonance Images for Individualized Head Modeling. *Neuroimage* **2020**, *219*, 117044. [\[CrossRef\]](#) [\[PubMed\]](#)
12. Piastra, M.C.; Van Der Crujisen, J.; Piai, V.; Jeukens, F.E.; Manoochchri, M.; Schouten, A.C.; Selles, R.W.; Oostendorp, T. ASH: An Automatic Pipeline to Generate Realistic and Individualized Chronic Stroke Volume Conduction Head Models. *J. Neural Eng.* **2021**, *18*, 044001. [\[CrossRef\]](#) [\[PubMed\]](#)
13. Ti, C.H.E.; Yuan, K.; Tong, R.K. TDCS Inter-Individual Variability in Electric Field Distribution for Chronic Stroke: A Simulation Study. In Proceedings of the 2021 10th International IEEE/EMBS Conference on Neural Engineering (NER), Online, 4–6 May 2021; pp. 1048–1051. [\[CrossRef\]](#)
14. Dmochowski, J.P.; Datta, A.; Huang, Y.; Richardson, J.D.; Bikson, M.; Fridriksson, J.; Parra, L.C. Targeted Transcranial Direct Current Stimulation for Rehabilitation after Stroke. *Neuroimage* **2013**, *75*, 12–19. [\[CrossRef\]](#) [\[PubMed\]](#)

15. Opitz, A.; Falchier, A.; Yan, C.-G.; Yeagle, E.M.; Linn, G.S.; Megevand, P.; Thielscher, A.; Deborah, A.R.; Milham, M.P.; Mehta, A.D. Spatiotemporal Structure of Intracranial Electric Fields Induced by Transcranial Electric Stimulation in Humans and Nonhuman Primates. *Sci. Rep.* **2016**, *6*, 1–11. [[CrossRef](#)] [[PubMed](#)]
16. Huang, Y.; Liu, A.A.; Lafon, B.; Friedman, D.; Dayan, M.; Wang, X.; Bikson, M.; Doyle, W.K.; Devinsky, O.; Parra, L.C. Measurements and Models of Electric Fields in the in Vivo Human Brain during Transcranial Electric Stimulation. *eLife* **2017**, *6*, e18834. [[CrossRef](#)]
17. Lafon, B.; Henin, S.; Huang, Y.; Friedman, D.; Melloni, L.; Thesen, T.; Doyle, W.; Buzsáki, G.; Devinsky, O.; Parra, L.C. Low Frequency Transcranial Electrical Stimulation Does Not Entrain Sleep Rhythms Measured by Human Intracranial Recordings. *Nat. Commun.* **2017**, *8*, 1–14. [[CrossRef](#)]
18. Vöröslakos, M.; Takeuchi, Y.; Brinyiczki, K.; Zombori, T.; Oliva, A.; Fernández-Ruiz, A.; Kozák, G.; Kincses, Z.T.; Iványi, B.; Buzsáki, G. Direct Effects of Transcranial Electric Stimulation on Brain Circuits in Rats and Humans. *Nat. Commun.* **2018**, *9*, 1–17. [[CrossRef](#)]
19. Louviot, S.; Tyvaert, L.; Maillard, L.G.; Colnat-Coulbois, S.; Dmochowski, J.; Koessler, L. Transcranial Electrical Stimulation Generates Electric Fields in Deep Human Brain Structures. *Brain Stimul.* **2022**, *15*, 1–12. [[CrossRef](#)]
20. Esmaeilpour, Z.; Milosevic, M.; Azevedo, K.; Khadka, N.; Navarro, J.; Brunoni, A.; Popovic, M.R.; Bikson, M.; Fonoff, E.T. Proceedings# 21. Intracranial Voltage Recording during Transcranial Direct Current Stimulation (TDCS) in Human Subjects with Validation of a Standard Model. *Brain Stimul. Basic Transl. Clin. Res. Neuromodulation* **2017**, *10*, e72–e75.
21. Chhatbar, P.Y.; Kautz, S.A.; Takacs, I.; Rowland, N.C.; Revuelta, G.J.; George, M.S.; Bikson, M.; Feng, W. Evidence of Transcranial Direct Current Stimulation-Generated Electric Fields at Subthalamic Level in Human Brain in Vivo. *Brain Stimul.* **2018**, *11*, 727–733. [[CrossRef](#)]
22. Datta, A.; Bikson, M.; Fregni, F. Transcranial Direct Current Stimulation in Patients with Skull Defects and Skull Plates: High-Resolution Computational FEM Study of Factors Altering Cortical Current Flow. *Neuroimage* **2010**, *52*, 1268–1278. [[CrossRef](#)]
23. Guidetti, M.; Arlotti, M.; Bocci, T.; Bianchi, A.M.; Parazzini, M.; Ferrucci, R.; Priori, A. Electric Fields Induced in the Brain by Transcranial Electric Stimulation: A Review of In Vivo Recordings. *Biomedicines* **2022**, *10*, 2333. [[CrossRef](#)]
24. Huang, Y.; Datta, A.; Bikson, M.; Parra, L.C. Realistic Volumetric-Approach to Simulate Transcranial Electric Stimulation—ROAST—A Fully Automated Open-Source Pipeline. *J. Neural Eng.* **2019**, *16*, 056006. [[CrossRef](#)] [[PubMed](#)]
25. McCann, H.; Pisano, G.; Beltrachini, L. Variation in Reported Human Head Tissue Electrical Conductivity Values. *Brain Topogr.* **2019**, *32*, 825–858. [[CrossRef](#)] [[PubMed](#)]
26. Tadel, F.; Baillet, S.; Mosher, J.C.; Pantazis, D.; Leahy, R.M. Brainstorm: A User-Friendly Application for MEG/EEG Analysis. *Comput. Intell. Neurosci.* **2011**, *2011*, e879716. [[CrossRef](#)] [[PubMed](#)]
27. Wang, M.; Feng, T.; Jiang, H.; Zhu, J.; Feng, W.; Chhatbar, P.Y.; Zhang, J.; Zhang, S. In Vivo Measurements of Electric Fields during Cranial Electrical Stimulation in the Human Brain. *Front. Hum. Neurosci.* **2022**, *16*. [[CrossRef](#)] [[PubMed](#)]
28. Datta, A.; Baker, J.M.; Bikson, M.; Fridriksson, J. Individualized Model Predicts Brain Current Flow during Transcranial Direct-Current Stimulation Treatment in Responsive Stroke Patient. *Brain Stimul.* **2011**, *4*, 169–174. [[CrossRef](#)]
29. Minjoli, S.; Saturnino, G.B.; Blicher, J.U.; Stagg, C.J.; Siebner, H.R.; Antunes, A.; Thielscher, A. The Impact of Large Structural Brain Changes in Chronic Stroke Patients on the Electric Field Caused by Transcranial Brain Stimulation. *NeuroImage Clin.* **2017**, *15*, 106–117. [[CrossRef](#)]
30. Johnstone, A.; Zich, C.; Evans, C.; Lee, J.; Ward, N.; Bestmann, S. The Impact of Brain Lesions on TDCS-Induced Electric Field Magnitude. *bioRxiv* **2021**. bioRxiv:19-436124.